NOVEL POSITIONS ESTIMATORS FOR TIMING BELT DRIVERS

Received 2nd April; accepted 21st April.

Ergin Kilic, Melik Dölen, Buöra Koku, Can Ulas Dogruer

Abstract:

This paper focuses on viable position estimation schemes for timing belt drives where the position of the carriage (load) is to be calculated via reference models accepting input from a position sensor on the actuator of the timing belt. A detailed analysis on the source of transmission errors is presented a number of relevant mathematical models are developed utilizing a priori knowledge on the process. The paper illustrates that such schemes are very effective when the drive system is not subjected to external loads as well as widely changing operating conditions such as ambient temperature, belt tension.

Keywords: *sensors, actuators, safety.*

1. Introduction

Timing belt drives are increasingly utilized to convert rotary motion into translation in high-precision motion-control systems, such as inkjet printers, plotters, specialized CNC machine tools (filament winding machines, rapid prototyping machines), vision systems, and some bio-medical equipment [1]. In such machines, the carriage housing a special apparatus is usually driven by an elastic transmission element like a timing belt. Thus, the linear motion of the apparatus must be controlled accurately via direct position measurements in order to attain the goals of the particular task at hand.

The main disadvantage of elastic elements in such arrangements is that they do introduce well-known non-linearities (such as friction, elasticity, backlash, time delay) to the servo loop [2]. Hence, advanced control schemes [1-6] must frequently accompany direct measurement/feedback techniques to achieve the desired precision and positioning accuracy.

It is critical to note that when the characteristic travel-span ("stroke") of a generic machine is quite high (> 0.5 m), the use of direct measurement techniques employing traditional sensors (such as potentiometers, LVDTs, linear scales, laser interferometers) leads to both bulky and relatively expensive solutions. Hence, the main motivation of this paper is to propose feasible estimation schemes that utilize the information emanating from a lowcost sensor on the pulley of the drive, so that the position of the carriage could be estimated to the desired accuracy for „not-so-demanding" applications.

The organization of the paper is as follows: after this brief introduction, the paper introduces the experimental setup along with a number accompanying tests to investigate the transmission characteristics of a generic timing belt drive. Based on the information collected, the paper makes a detailed analysis on the source of position errors. Consequently, three (kinematic) models are presented in the following section. The next article illustrates the estimation performance of the proposed models. Finally, the key points of the paper are discussed in detail.

2. System and tests

To study transmission error attributes of generic timing belt drives, the linear stage of a CMM that was initially designed within the framework of a senior capstone design course (ME 407) has been adapted. Figure 1 illustrates this setup where a DC motor with a built-in gearbox drives the carriage via a timing belt. A schematic of this setup is also given in Figure 2 while Table 1 tabulates important elements employed in the arrangement.

For modeling and verification purposes, a high-resolution linear scale (LS) is integrated into the setup. Notice that in this setup, since it is desirable to control the acceleration/ deceleration of the carriage accurately, a custom motion controller is utilized in the system.

Table 1. The summary of elements used in the experi-mental setup.

Elements	Type / Model	Remarks
Motor	150 W Brush-type DC motor	Built-in gearbox (23.7222:1)
Motor Driver	Trans-conductance amplifier	800 W / MOSFET
Timing Belt	General purpose	Pitch: 5.08 mm (0.2")
Controller	PIC16F877A @ 20 Mhz	8-bit RISC controller
Motor Encoder	Autonics ENB quadrature optical encoder	2000 pulses/rev (ea. quad. channel)
Linear Scale	Heidenhain LS-176C (Distance coded)	500 pulses / mm (ea. quad. channel)
Data Acquisition Board	Humusoft MF-614	4 enc. inputs, 4 DAC, 16 ADC, 8 DI, 8 DO.
Software	Matlab Real-time Windows Target	Data capture, analysis, and visualization

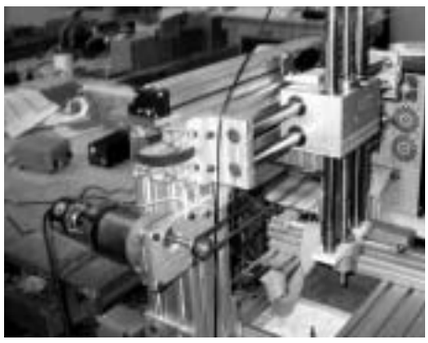

Figure 1. General view of the setup.

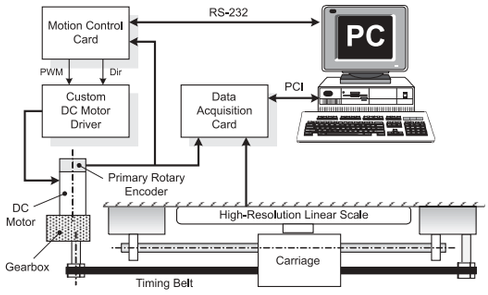

Figure 2. Schematic of experimental setup.

To determine the displacement errors introduced by the transmission system, the position measurements of the primary encoder (PE) are to be compared to those of the high-resolution linear scale that is directly coupled to the carriage of the linear stage. Unfortunately, the measurement axes of the LS and that of the PE could not coincide due to the limitations imposed by the physical layout of the stage. Therefore, as shown in Figure 3, the Abbe offset errors will be indirectly included to the observed displacement errors.

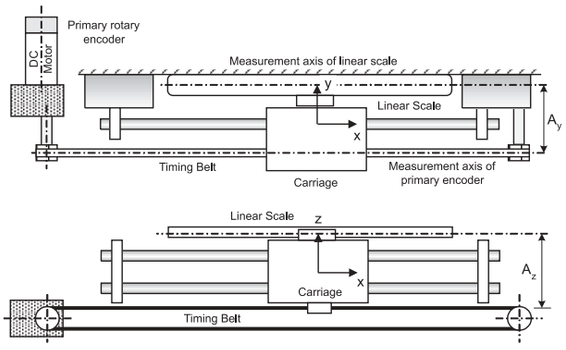

Figure 3. Abbe offsets.

That is, the difference between the measurements takes the following form:

$$\Delta x = x_{LS} - x_{PE} = \delta_x(x_{PE}) + A_z\varepsilon_y(x_{PE}) - A_y\varepsilon_z(x_{PE}) \quad (1)$$

where x_{LS} and x_{PE} refer to the position measurements of the LS and PE respectively. Here,

$A_y, A_z \equiv$ Abbe offsets (positive);

$\varepsilon_y, \varepsilon_z \equiv$ Small angular rotations about principal axes;

$\delta_x \equiv$ Displacement error introduced by the transmission system.

Since Δx in (1) constitutes the geometric / kinematic errors associated with support elements (anti-friction bearings, bearing shafts); the transmission error, which is the primary focus of this study, has to be isolated via relevant transformations.

3. Experiments

Within the scope of this study, several tests are conducted. First of all, the repeatability of the motion must be studied as a prerequisite to devise reliable reference models. In all tests considered, the motor's velocity is accurately controlled along a trapezoidal path as shown in Figure 4 where the resulting (position) tracking error in Figure 5 (that essentially go to zero at the steady state) can be assumed low for all intensive purposes. Under the above-mentioned conditions, the positioning error patterns ($\Delta x = x_{LS} - x_{PE}$) for twelve different (overlaid) trajectories are illustrated in Figure 6. As can be verified frequency chart in Figure 7, the positioning errors, which exhibit hysteresis character, are quite repeatable which in turn encourages the development of advanced estimator models.

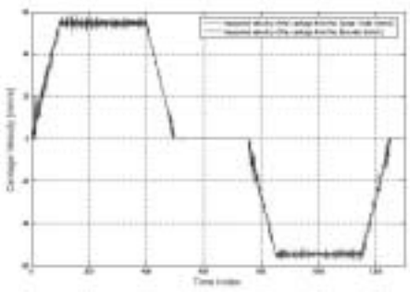

Figure 4. Velocity profile of the carriage.

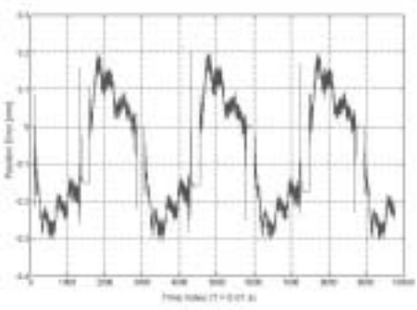

Figure 5. Position tracking error.

In fact, the close examination of the error patterns in Figure 6 reveals critical points about the attributes of the system under investigation:

- Hysteresis band, which is roughly 0.3 mm for the test cases, is apparently a consequence of the backlash between the timing belt and the driving pinion. A dramatic increase in the belt tension tends to widen this band as the gap between the teeth gets stretched out.
- As mentioned earlier, the Abbe offset errors manifest themselves as the waveforms on the upper and lower boundaries. Hence, mechanical manipulations on the bearing elements usually impress a different texture on these bounds.

- Fundamental harmonic components (with a magnitude of 10 microns) superimposed onto the band are at the tooth-passing frequency of the belt and thus the observed variations could be mainly attributed to form errors of the belt.
- Harmonics injected by the two-stage gearbox of the motor appear to be quite negligible while the transition in the backlash zone (of which has bandwidth of 0.12 mm) is extremely fast when a change in the direction of motion is observed.

The next set of experiments focuses on the effect of velocity on the transmission error. Figure 8 illustrates five different displacement errors along full travel span of the mechanism. As can be seen, dramatic changes at the steady state velocity does have only minor influences on the nature of the nonlinear relationship.

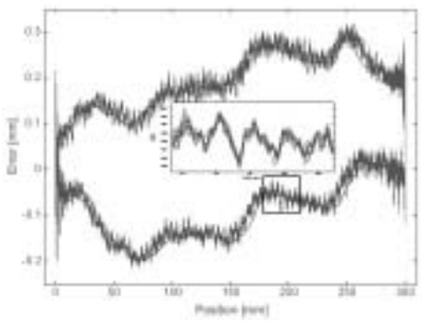

Figure 6. Position errors for 12 cases.

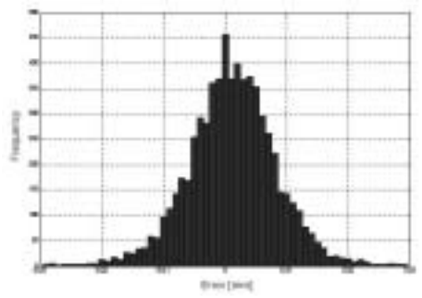

Figure 7. Frequency of positioning errors.

Finally, the effect of inertial forces is investigated by modifying the acceleration and deceleration profile of the controlled motor such that the sliding motion inside the hysteresis band is induced under the action of these inertial forces. As can be seen from Figure 9, the inertial forces do not have a considerable effect on the closing distances. Similarly, Figure 10 elaborates the closing distances when the direction of motion is reversed at various intermediate locations. It is interesting to note that when the direction of travel is reversed, the power transmitting teeth disengage and micro-slip under external excitation comes into play. Consequently, the belt slowly slides until the next set of teeth pairs engage into transmission. Unfortunately, developing dynamic models that explain the observed phenomena satisfactorily is known to be quite challenging and is an active research field in tribology [7].

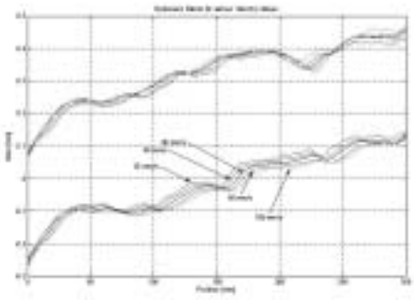

Figure 8. Low-pass filtered displacement errors for various steady-state velocities.

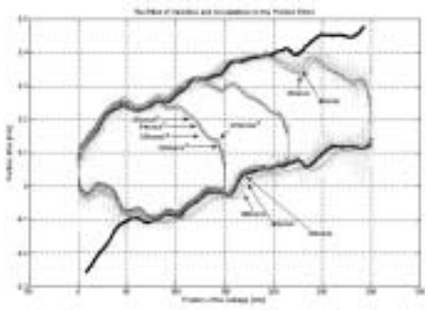

Figure 9. Effect of acceleration/deceleration on displacement errors.

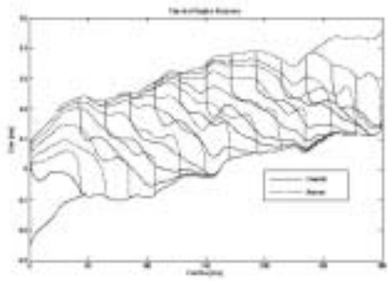

Figure 10. Position errors on motion reversals at various intermediate locations.

4. Kinematic models of timing belt mechanism

Despite their common use in precision machinery, the transmission characteristics of elastic transmission elements have not been fully evaluated in the literature. Hence, a simple (yet effective) kinematic model is to be devised within the scope of this study. As shown in the Figure 11, the motor driving the belt is characterized by an ideal rack-and-pinion mechanism. Similarly, the backlash associated with the built-in gearbox of the motor is modeled by a slider mechanism where an ideal camshaft inside the mechanism accounts for the changing hysteresis band ($h_g = L_g - P_g$) because of different form/surface errors on transmitting teeth pairs. Likewise, the other slider mechanism in the model stands for the hysteresis nonlinearity ($h_b = L_b - P_b$) of the timing belt. Figure 12 shows the block diagram of the resulting system. If the harmonics injected by both gearbox and timing belt are to be neglected for the sake of simplicity, the system conveniently boils down to a single hysteresis loop. This simplification can be also verified through the experimental data presented in the previous section.

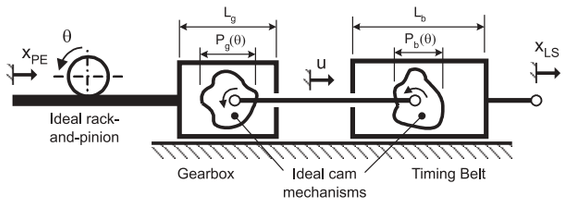

Figure 11. Kinematic model of the timing belt drive.

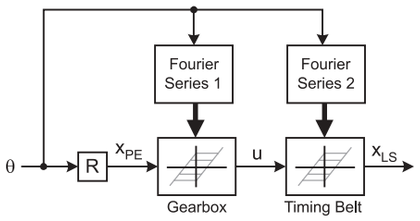

Figure 12. Block diagram of the proposed model.

Unfortunately, the trajectories being followed inside the band can be quite complicated owing to the fact that the micro-slip process, which cannot be described satisfactorily, becomes dominant in the region. Instead of developing sophisticated dynamic models (with a large number of free parameters), a more pragmatic approach is to be followed in the paper. In fact, the trajectories presented in Figure 10 encourage the development of three models with different physical meanings and computational costs. The descriptions of these models follow.

4.1 Model 1: Linear Transition

Hysteresis band model shown in the Figure 13 is first considered. Depending on the direction of travel (x) as well as the position registered when the direction has changed, a linear path is traversed inside the band as

(2)

$$y(k)=\begin{cases} m\cdot x(k)-h, & x(k)\geq x(k-1) \\ u(k)=y_d(k)-a\left[x(k)-x_d(k)\right] & \left[x(k)\geq x(k-1)\right]\wedge\left[u(k)\geq m\cdot x(k)-h\right] \\ m\cdot x(k), & x(k)<x(k-1) \\ u(k)=y_d(k)-b\left[x(k)-x_d(k)\right] & \left[x(k)<x(k-1)\right]\wedge\left[u(k)<m\cdot x(k)\right] \end{cases}$$

Here, a, b, m denote the slope of various lines while h indicates the hysteresis band. In this expression, k is time index; $x(k)$ is primary encoder position at $t = kT$ while $y(k)$ denotes position error at $t = kT$. Note that x_d and y_d correspond to the primary encoder position and the error when a direction change has been registered:

(3)

$$x_d(k)=\begin{cases} x(k-1), & \left\{\left[x(k)\geq x(k-1)\right]\wedge\left[x(k-1)<x(k-2)\right]\right\} \\ & \vee\left\{\left[x(k)<x(k-1)\right]\wedge\left[x(k-1)\geq x(k-2)\right]\right\} \\ x_d(k-1), & else \end{cases}$$

(4)

$$y_d(k)=\begin{cases} y(k-1)-h_g, & \left\{\left[x(k)\geq x(k-1)\right]\wedge\left[x(k-1)<x(k-2)\right]\right\} \\ y(k-1)+h_g, & \left\{\left[x(k)<x(k-1)\right]\wedge\left[x(k-1)\geq x(k-2)\right]\right\} \\ y_d(k-1), & else \end{cases}$$

4.2 Model 2: Exponential Transition

As a second case, the model in Fig 14 is taken into consideration. In this model, when the direction has changed, an exponential path is traversed in the loop as

(5)

$$y(k)=\begin{cases} m\cdot x(k)-h, & x(k)\geq x(k-1) \\ u(k)=y_d(k)-A\left[1-e^{a\left[x(k)-x_d(k)\right]}\right] & \left[x(k)\geq x(k-1)\right]\wedge\left[u(k)\geq m\cdot x(k)-h\right] \\ m\cdot x(k), & x(k)<x(k-1) \\ u(k)=y_d(k)+B\left[1-e^{-b\left[x(k)-x_d(k)\right]}\right] & \left[x(k)<x(k-1)\right]\wedge\left[u(k)<m\cdot x(k)\right] \end{cases}$$

Here, A, B, a, b denote the parameters of the exponential curves while x_d and y_d are as defined in (3) and (4).

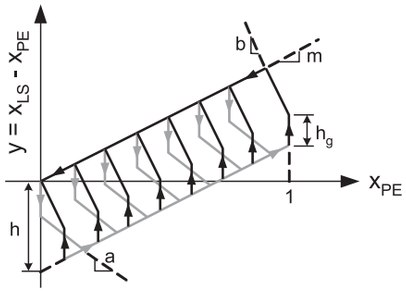

Figure 13. Linear transition model.

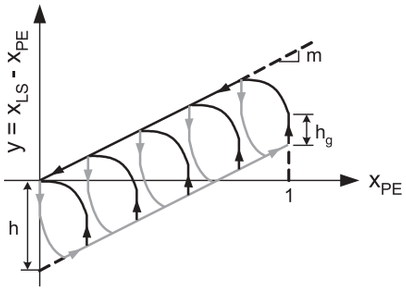

Figure 14. Exponential transition model.

4.3 Model 3: Linear Interpolation

As a third or more general case, a linear interpolation model representing the transitions inside the hysteresis band is considered:

(6)

$$y(k)=\begin{cases} \Lambda_f(x(k)), & x(k)\geq x(k-1) \\ u(k)=\Lambda_{fi}(x(k),x(k-1),x_d(k),y_d(k)), & \left[x(k)\geq x(k-1)\right]\wedge\left[u(k)\geq m\cdot x(k)-h\right] \\ \Lambda_r(x(k)), & x(k)<x(k-1) \\ u(k)=\Lambda_{ri}(x(k),x(k-1),x_d(k),y_d(k)), & \left[x(k)<x(k-1)\right]\wedge\left[u(k)<m\cdot x(k)\right] \end{cases}$$

where Λ_f, Λ_r indicates the lookup table for the lower and upper band respectively while Λ_f and Λ_r denote multi-dimensional lookup tables created using the transient data presented in Figure 10.

5. Results and discussion

To make a comparative evaluation among the presented model, the free parameters of the models are to be determined using the relevant experimental data *via* least squares method. Table 2 tabulates these parameters.

Table 2. Model parameters.

Motor	m	h	h_g	a	b	A	B
1: Linear	0.0010594	0.34	0.11	0.0012	0.0012	–	–
2: Exponential	0.0010594	0.34	0.11	-0.05	-0.03	0.07	0.09

With respect to the third (interpolation) model, the relevant parameters are inherited from those of the linear model while two-dimensional lookup table (with a total 650 data points) are formed utilizing the characteristic curves in Figure 10.

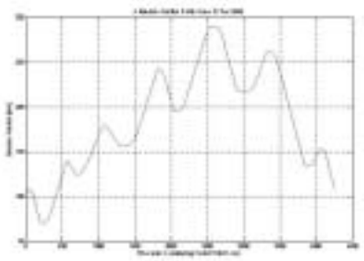

Figure 15. Test scenario.

Once the models and the lookup tables are formed, the estimation performances of all the models are assessed through a complicated case scenario where the carriage abruptly changes its direction through its course as illustrated in Figure 15. The estimation results are presented in Figs. 16 through 21. Similarly, Table 3 summarizes the statistics of the resultant data.

Table 3. Summary of results.

μ(m)	Model 1	Model 2	Model 3	Model 4
Max	131	120	99	365
Min	-148	-130	-79	-93
RMS	38	34	26	195

Note that in Table 3, the root-mean-square error is defined as

$$e_{rms} = \sqrt{\frac{1}{K}\sum_{k=1}^{K}\left[x_{LS}(k) - x_{PE}(k) - y(k)\right]^2} \qquad (7)$$

The performances of Model 1 and 2 are very close to each other owing to the fact that the fit curves are quite similar. As expected, linear interpolation yields the performance as the data used to form the lookup tables essentially captures the essence of the transition region.

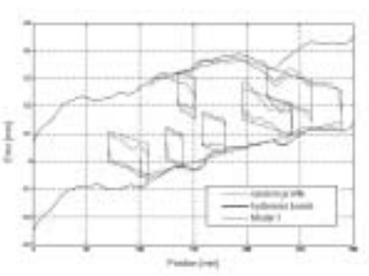

Figure 16. Estimation performance of Model 1.

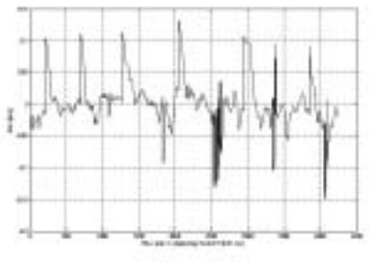

Figure 17. Error profile of Model 1.

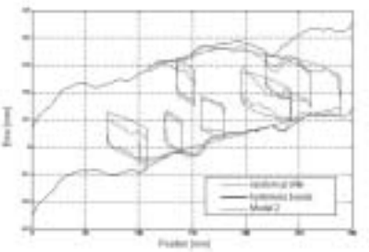

Figure 18. Estimation performance of Model 2.

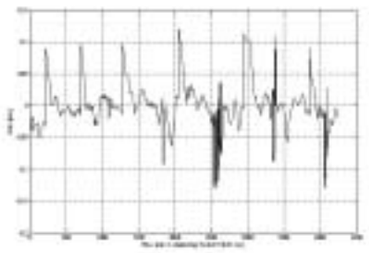

Figure 19. Error profile of Model 2.

6. Conclusion

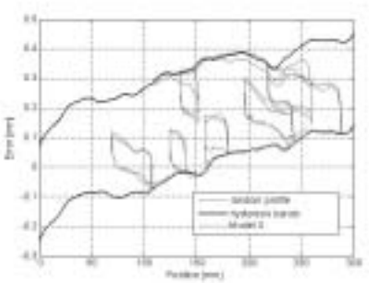

Figure 20. Estimation performance of Model 3.

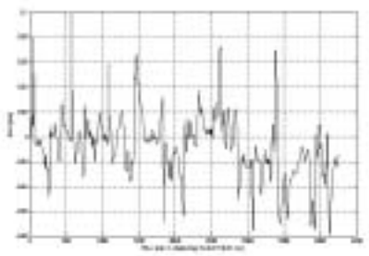

Figure 21. Error profile of Model 3.

The paper proposes three different hysteresis models for timing belt drives. The study illustrates that advanced estimation schemes are quite effective when the drive system is not subjected to external loads as well as widely changing operating conditions such as ambient temperature and belt tension.

ACKNOWLEDGMENTS

This work has been partially supported by the Turkish Scientific and Technical Research Council (TÜBİTAK) under the project MISAG-257 and partially by METU/BAP under contract

AUTHORS

Ergin Kilic and **Buöra Koku** – Middle East Technical University, Department of Mechanical Engineering, Ankara, 06531, Turkey.

Melik Dölen*– Middle East Technical University, Department of Mechanical Engineering, Ankara, 06531, Turkey. Tel. [+90] (312) 210-5272, Fax: [+90] (312) 210-2536, e-mail: dolen@metu.edu.tr.

Can Ulas Dogruer – Hacettepe University, Department of Mechanical Engineering, Ankara, 6800, Turkey.

* corresponding author

References

[1] A. S. Kulkarni, and M. A. El-Sharkawi "Intelligent Precision Position Control of Elastic Drive Systems," *IEEE Trans. On Energy. Conv.*, vol 16:1, 2001, pp 26-31.

[2] W. Li and M. Rehani, "Modeling and control of a belt-drive positioning table," in: *Proceedings of the 22nd IEEE International Conference of Industrial Electronics (IECON)*, vol. 3, Taipei, Taiwan, Aug. 1996, pp. 1984–1989.

[3] Z. Zhao and L. Cai, "On the improvement of tracking performance of positioning tables," in: *Proc. of the 22nd IEEE International Conference of Industrial Electronics (IECON)*, vol. 3, Taipei, Taiwan, 1996, pp. 1990–1995.

[4] S. Abrate, "Vibrations of belts and belt drives," *Mechanism and Machine Theory*, vol. 27, no. 6, pp. 645–659, 1992.

[5] D. W. South and J. R. Mancuso, Eds., *Mechanical Power Transmission Components*. New York: Marcel Dekker Inc., 1994.

[6] E. Ostertag and M. J. Carvalho-Ostertag, "Fuzzy control of an inverted pendulum with fuzzy compensation of friction forces," *International Journal of Systems Science*, vol. 24, no. 10, 1993, pp. 1915–1921.

[7] B. Armstrong-Helouvry, P. Dupont, and C. Canudas De Wit, "A survey of models, analysis tools and compensation methods for the control of machines with friction," *Automatica*, vol. 30, no. 7, 1994, pp. 1083–1138.